Molecular Dynamics simulations of initial Pd and PdO nanocluster growths in a magnetron gas aggregation source

Pascal Brault, William Chamorro-Coral, Sotheara Chuon, Amaël Caillard, Jean-Marc Bauchire, Steve Baranton, Christophe Coutanceau, Erik Neyts

Molecular Dynamics simulations of initial Pd and PdO nanocluster growths in a magnetron gas aggregation source

Pascal Brault[1,(✉)], William Chamorro-Coral[1], Sotheara Chuon[1], Amaël Caillard[1], Jean-Marc Bauchire[1], Stève Baranton[2], Christophe Coutanceau[2], Erik Neyts[3]

[1]GREMI UMR 7344 CNRS – Université d'Orléans, BP6744 45067 Orléans Cedex 2, France
[2]IC2MP UMR 7285 CNRS – Université de Poitiers, TSA 51106, 86073 Poitiers cedex 9, France
[3]Department of Chemistry, University of Antwerp, Research group PLASMANT, Universiteitsplein 1, 2610 Antwerp, Belgium

✉ Pascal Brault, pascal.brault@univ-orleans.fr

Abstract: Molecular dynamics simulations are carried out for describing growth of Pd and PdO nanoclusters using the ReaxFF force field. The resulting nanocluster structures are successfully compared to those of nanoclusters experimentally grown in a gas aggregation source. The PdO structure is quasi-crystalline as revealed by HRTEM analysis for experimental PdO nanoclusters. The role of the nanocluster temperature in the MD simulated growth is highlighted.

Keywords: Molecular dynamics, cluster growth, plasma sputtering, nanocatalyst

1. Introduction.

Nanoparticles (NPs) play a central role in many applications. Among them catalysis represents certainly a broad field of uses [1]. The open questions are centered on the capability of producing nanoclusters with well-defined size and shape distributions. Physical Vapor Deposition (PVD) techniques are now mature synthesis methods able to reach such goals [2]. Among all possible PVD techniques, the magnetron gas aggregation has rapidly become a widely used technique due to its simplicity and its convenience to allow the growth of a large kind of metallic and metal-oxide nanoparticles [3-18]. Despite numerous studies on particle growth, either experimental or theoretical/numerical as reviewed in Ref. 18, very few of them take into account the reactivity at the molecular level under conditions matching those of experimental syntheses of NPs.

Molecular Dynamics simulation (MDs) is a very efficient technique for describing atomic and molecular processes, especially at the nanoscale. It consists in solving the equation of motion using Newton equations of motion (or Langevin dynamics which includes energy dissipation through an additional friction term):

$$\frac{\partial^2}{\partial t^2}\vec{r_{\mathrm{i}}} = \frac{1}{m_{\mathrm{i}}}\vec{f_{\mathrm{i}}}, \qquad \vec{f_{\mathrm{i}}} = -\frac{\partial}{\partial r} V(\vec{r}_1(t), \vec{r}_2(t), \cdots, \vec{r}_{\mathrm{N}}(t)) \qquad (1)$$

where $\vec{r}_{\mathrm{i}}(t)$ is the position of the atom i belonging to an assembly of N atoms, at a time *t* and with a mass m_{i}, and *V* is the interaction potential between all atoms. So solving such a set of equations requires the knowledge of the interaction potentials *V* and a set of initial conditions, preferably matching experimental situations

Moreover, recent developments now enable MD to treat molecular reactions allowing a direct comparison with experiments. This means that bond formation and bond breaking can be described. A widely used force field for achieving this goal is ReaxFF, which also includes variable partial charges allowing to study reactivity in ionic systems [19]. Additionally, both

these force fields are including variable partial charges, increasing their interest in studying reactivity of ionic systems.

Palladium and palladium oxide NPs are of very high interest for catalytic combustion [20,21] and more recently for the conversion of biomass molecules into hydrogen and added-value compounds [22-25]. In this context, the present study examines the MDs of the growth of Pd and PdO NPs in conditions matching those of the Gas Aggregation Source (GAS) setup. The theoretical structures of Pd and PdO NPs as calculated using MDs are compared with those determined from high resolution transmission electron microscopy pictures of experimentally grown PdO using a GAS setup.

2. Methods

The GAS setup (MANTIS Deposition Ltd) was previously fully described in Ref. 6. The scheme of Fig. 1 represents the working principle of the GAS. Pd atoms are sputtered from a Pd target (Lesker, 99.99% purity in a condensation chamber filled by a mixture of argon gas at a pressure of 38 Pa and a 100 sscm flow rate, and oxygen gas at a flow rate of 5 sccm. Magnetron sputtering is ignited by electrical breakdown of the Pd target biased at negative voltage V_b = -400 V. Growth of Pd and PdO clusters occurs in the condensation chamber and the clusters are leaving the condensation chamber via an outlet orifice with a diameter of 5 mm towards a differentially pumped deposition chamber. The nanoclusters are collected onto carbon-coated Cu grids (300 mesh, SPI) and analyzed on high resolution transmission microscope (HRTEM) JEM – ARM 200F Cold FEG TEM/STEM operating at 200 kV and equipped with a spherical aberration (Cs) probe and image correctors (point resolution 0.12 nm in TEM mode).

.

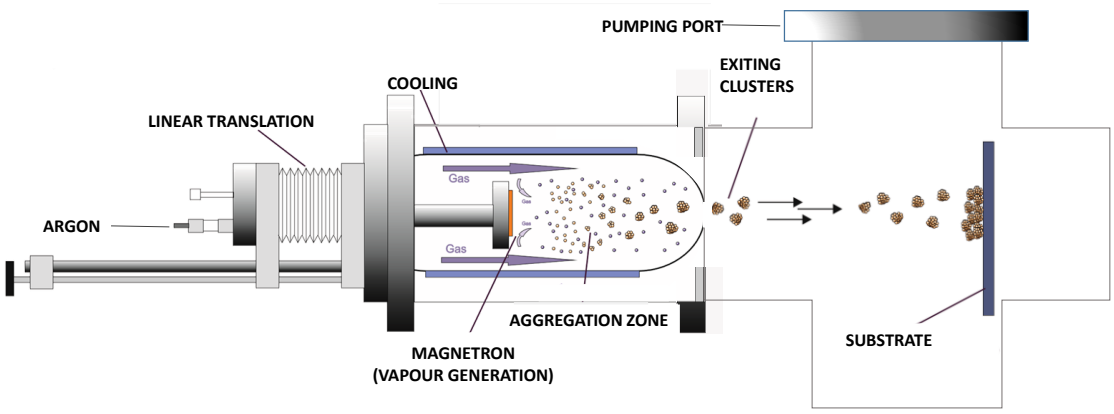

Figure 1: *Scheme of the working principle of the Gas Aggregation Source setup.*

Molecular dynamics simulations of cluster growth are carried out using PdO ReaxFF potentials [26]. Ar-Pd and Ar-O interactions are described using Molière potentials [27]. The simulation box is representative of the GAS conditions. The Pd to Ar, and O to Ar ratios are estimated using the procedure described by Quesnel et al. [9]. This leads to a simulation box containing 20,000 Ar atoms, 500 Pd atoms and 0 to 1,000 O atoms. The initial temperature of this vapor is T_{gas} = 300 K. Initial velocities of atoms are sampled from a Maxwell-Boltzmann distribution at 300 K. Moreover, while all calculations are performed considering a constant number of atoms, constant volume and constant total energy (NVE) ensemble, while using NVT ensemble (Temperature of Ar atoms is constant instead of E) for the Ar atoms, mimicking cluster cooling via Ar collisions on clusters and transport to chamber wall. Atoms are initially randomly located in a periodic simulation box of 40 x 40 x 40 nm^3. These initial values are deduced from the actual conditions used for the experimental cluster growth processes in the GAS setup, and it is expected that they allow a relevant comparison with HRTEM observations of real clusters. The simulations are continued up to a simulated time of 25 ns, corresponding to $1.00x10^8$ time-steps (the integration time-step is fixed to 0.25 fs, according to Ref. 26). All simulations are carried out using the LAMMPS software[1] [28].

3. Results and discussion

[1] https://lammps.sandia.gov

Fig. 2 displays snapshots of Pd growth at 25 ns elapsed calculation time in the absence (Fig. 2a) and in the presence (Fig. 2b) of oxygen. Ar atoms are not represented for clarity.

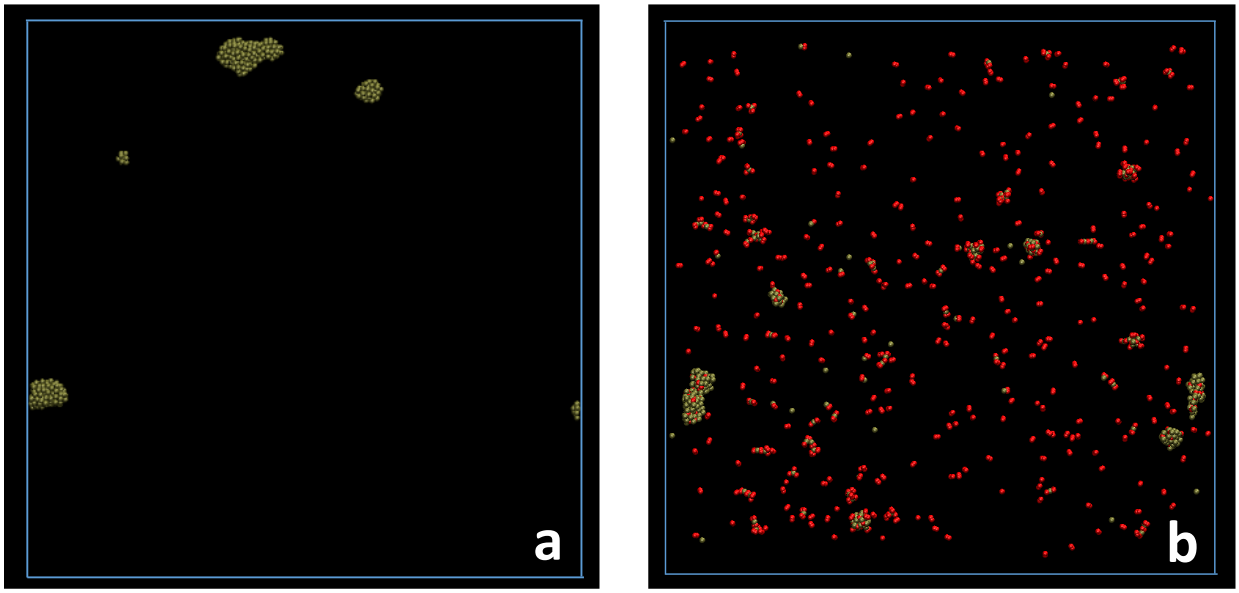

Figure 2: *Snapshots at 25 ns calculation time for the growth of (a) Pd clusters considering 20,000 Ar atoms (not shown for clarity), 500 Pd atoms and (b) of PdO_x considering 20,000 Ar atoms (not shown for clarity), 500 Pd atoms and 500 O_2 molecules (right panel). Pd atoms are colored green and unreacted O_2 molecules are colored red.*

In the case of the formation of Pd clusters (Fig. 2a), no isolated Pd atoms remains after 25 ns: all Pd atoms are incorporated in the formed clusters. Four clusters are present, containing 286, 159, 45 and 10 atoms. Indeed, considering the boundary conditions, the two pseudo-clusters visible close to the bottom of Fig. 2a belong to the same cluster. According to the RDF plot in Fig. 3, the Pd clusters appear well organized and crystalline. The interatomic distances between a Pd atom and the four nearest neighbor atoms (NNA) determined from the RDF plot are very close to the theoretical ones for Pd bulk (Table 1), which confirms the crystalline nature of the Pd clusters obtained by MD simulations.

Table 1. *Interatomic distances between a Pd atom and the four nearest neighbor atoms (NNA) in Pd clusters determined from the RDF plot (Fig. 3) and theoretical ones in Pd bulk.*

	Position (Å)			
	1st NNA	2nd NNA	3rd NNA	4th NNA
Pd Cluster	2.75	4.05	4.70	5.50
Pd Bulk	2.75	3.89	4.76	5.50

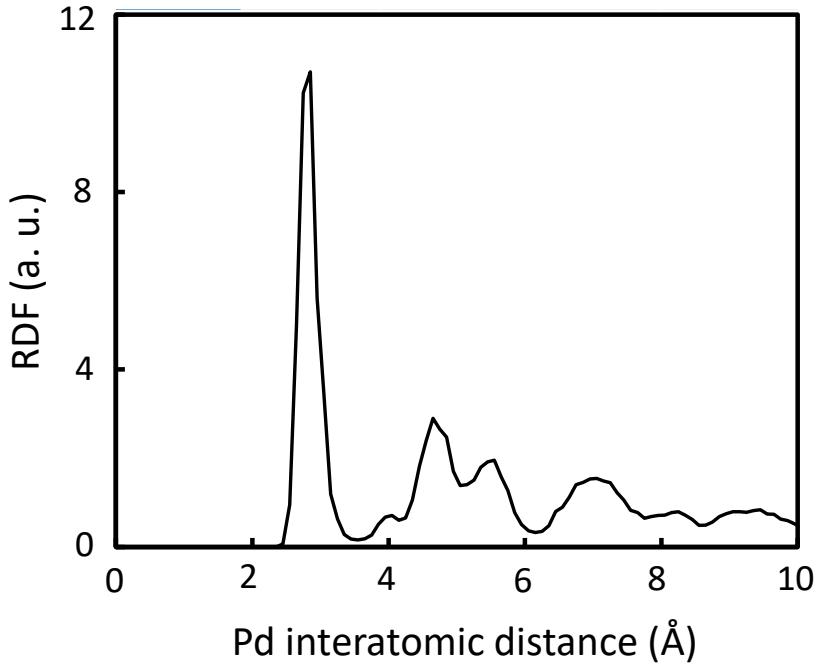

Figure 3: *RDF plot of Pd nanoclusters of Fig. 2.*

Another important point concerns the Pd vapor-cluster temperature change during the cluster growth. Fig. 4 displays the change in temperature of the Pd (red curve) and PdO_x (black curve) vapor-cluster for 25 ns of the MD simulations. In the case of Pd clusters, the temperature first increases during the growth of initial clusters. This temperature is controlled by the Pd sticking while the Pd dimer, trimer, etc. bond energy is removed by Ar atoms acting as a third body collision partner. When the clusters reach a sufficient size, they are able to store part of the bond energy issued from the sticking of an additional Pd atom. A maximum temperature is then reached when coalescence of atoms leads to clusters sufficiently big to be cooled by the argon collisions. Further, the cluster temperature decreases down to the argon temperature (300 K in

the present case) while collisions and coalescence of clusters become rare events. Bumps after 15 ns correspond to the coalescences of two clusters. At 25 ns, the remaining Pd nanoclusters are fully thermalized.

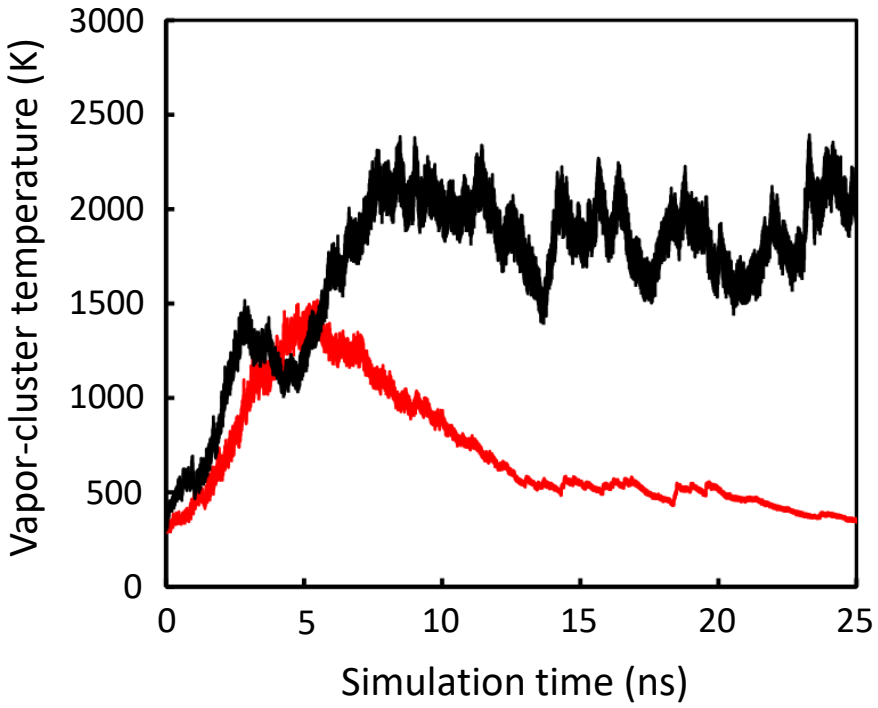

Figure 4: *Pd vapor (red curve) and Pd_xO_y in Pd/O_2 vapor (black curve) temperatures changes for the growth of Pd nanoclusters and Pd_xO_y nanoclusters.*

When adding O_2 to the Ar sputtering gas, the cluster growth is affected in numerous ways. When looking at the snapshot in Fig. 2b, Pd clusters are partly oxidized and do not appear well crystallized after 25 ns simulation time. Moreover 55% of the initial O_2 molecules are not inserted in or adsorbed on clusters, and remain at this step as unreacted molecules in the environmental atmosphere. The comparison of the snapshot for the formation of Pd clusters in the presence of O_2 molecules (Fig. 2b) with that for the formation of Pd clusters in the absence of O_2 molecules (Fig. 2a) indicates clearly that the number of clusters is higher in the presence of O_2 molecules than in their absence. Non-negligible amounts of PdO_x and Pd_2O_x small molecules can also be seen. This indicates that the clustering process needs more time in the presence of dioxygen than in its absence. This is confirmed by looking at the change of the vapor temperature of the Pd_xO_y species (O_2 molecules are excluded from the temperature

calculation) in Fig. 4 (black curve). As for the formation of Pd clusters, the temperature first increases due to the formation of Pd-Pd chemical bonds. This process is followed by a short decrease of the temperature at a time close to that for pure Pd clusters, indicating that Pd clusters are not so highly oxidized at this step. At longer times, an increase of temperature is observed, which is due to the formation of a significant amount of Pd-O bonds. The formation of such chemical bond releases a higher energy than that for the formation of a Pd-Pd chemical bond, i.e. about 1.3 eV for O adsorption on Pd and between 0.5 and 1 eV for Pd adsorption on Pd [26]. Afterwards, the temperature oscillates but does not decrease, despite the 20,000 Ar atoms thermostating the Pd_xO_y clusters and the remaining O_2 molecules. These oscillations of temperature are related to the collision and coalescence of smaller cluster into bigger ones. This means that longer computation time is necessary to obtain fully thermalized Pd_xO_y clusters. On the other hand the cluster composition has not yet reached the stable PdO stoichiometric composition. The larger Pd_xO_y clusters exhibit an O/Pd ratio of 0.25 to 0.3, while smaller clusters are rather molecules of the form PdO_x and Pd_2O_x. This is also an indication that the clustering process is slower for Pd_xO_y than for Pd for which, for the same computation time of 25 ns, no isolated Pd atom, dimers, trimers, etc. remained in the gas phase.

Nevertheless, one of the clusters in Fig. 2b has a nearly stoichiometric composition of $Pd_{21}O_{23}$. Fig. 5 depicts the atomic structure of this cluster. It is clearly observable that this cluster exhibits a nascent typical alternate Pd-O layered structure with the stoichiometry of pure PdO. This observation indicates that the formation of stoichiometric and crystalline PdO clusters can be expected for longer simulation times, i.e. when clusters will start to thermalize.

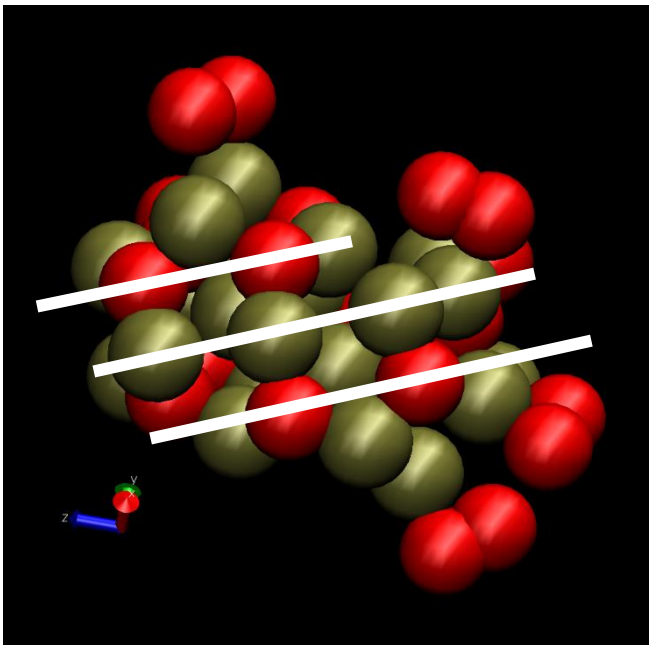

Figure 5: *Snapshot of a $Pd_{21}O_{23}$ cluster issued from figure 2. White lines underline the nascent Pd-O alternate layers. O_2 molecules at the cluster edges are adsorbed molecules.*

In order to compare the clusters obtained experimentally in the GAS set up experiments to those obtained from the MD simulations, which included starting conditions matching the experimental ones, HRTEM micrographs of a PdO experimental cluster were taken (Fig. 6a). The zoom in Fig. 6b and the Selected Area Electron Diffraction (SAED) pattern along the [010] axis (inset of Fig. 6b) reveal that we are in the presence of a PdO cluster. This is confirmed by the interplanar spacing of 0.266 nm and 0.156 nm and the angle between planes of around 30° corresponding to the {101} and {103} crystallographic planes of the PdO phase. In the micrograph it is also possible to observe the presence of 2D crystal defects as stacking faults and twin boundaries. The zoomed-in portion of the micrograph (Fig. 6b) shows clearly the position of the Pd atoms (oxygen are light atoms that are not detected) that matches the body centered tetragonal (bct) structure of PdO as shown in the schematic. The SAED pattern along the [010] zone axis shows a PdO crystal with a good crystal quality. The presence of oxygen introduces internal strains that deform the Pd crystal cell, as observed by the increase of the Pd-Pd interatomic distance (Table 1). Oxygen addition also increases the 2D defects due to the PdO formation.

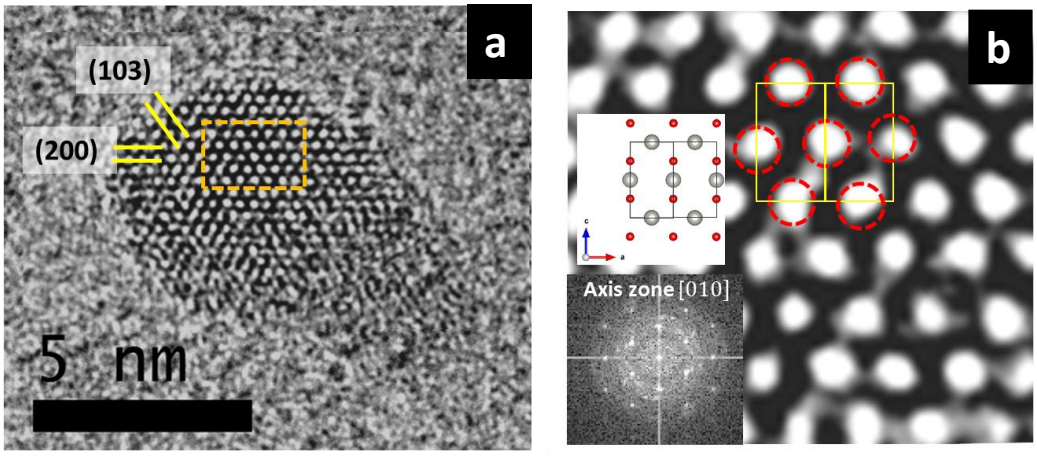

Figure 6: *HRTEM micrograph showing (a) an isolated PdO cluster with a size of 7 nm and (b) Zoom with a draw of the PdO crystal cell. Inset PdO SAED pattern along the [010] zone axis.*

Therefore, the structure of the experimentally obtained PdO nanoclusters using the GAS setup is fully in agreement with that foreseen using MD simulation based on initial conditions matching those of experimental synthesis. This indicates clearly that MD simulation is a very powerful method to predict the growth mechanism and structure of metal and metal oxide nanoparticles.

4. Conclusion

Reactive molecular dynamics simulations are carried out for describing the initial steps of the formation of Pd and PdO nanoclusters under conditions mimicking those for the growth of clusters in a magnetron gas aggregation source setup. When the formation of Pd clusters is carried out in the absence of O_2, the clustering process is complete at 25 ns simulation time. When adding oxygen in the sputtering gas clustering process is incomplete and small molecules such as PdO_x and Pd_2O_x are numerous; moreover 55% of the O_2 molecules did not react. This leads to kinetics of PdO_x cluster growth considerably slower than that of Pd cluster growth. Pd oxide NPs are observed with an O/Pd ratio close to 0.25 – 030. Nevertheless, stoichiometric PdO nanoclusters are also observed, which exhibit a nascent crystalline structure, while the cluster temperature of around 2000 K does not allow exhibiting a relaxed crystalline structure. On the other hand, experimental cluster formation in magnetron gas aggregation source setup

performed under comparable experimental conditions as those used in the simulations leads to the observation by HRTEM of stoichiometric and crystalline PdO nanoclusters.

Acknowledgments
Part of this work has been funded by French “Agence Nationale de la Recherche” under grant ANR-16-CE29-0007

References

[1] Tao F, RSC Catalysis Series No. 17, Metal Nanoparticles for Catalysis: Advances and Applications. Cambridge: Royal Society of Chemistry 2014

[2] Brault P. Review of Low Pressure Plasma Processing of Proton Exchange Membrane Fuel Cell Electrocatalysts. Plasma Processing and Polymers, 2016, 13:10–18

[3] Wegner K, Piseri P, Vahedi Tafreshi H and Milani P. Cluster beam deposition: a tool for nanoscale science and technology. Journal of Physics D: Applied Physics, 2006, 39:R439–R459

[4] Marek A, Valter J, Kadlec S and Vyskočil J. Gas aggregation nanocluster source ? Reactive sputter deposition of copper and titanium nanoclusters. Surface and Coatings Technology, 2011, 205:S573-S576

[5] Ayesh A I. Production of metal-oxide nanoclusters using inert-gas condensation technique Thin Solid Films, 2017, 636:207-213

[6] Caillard A, Cuynet S, Lecas T, Andreazza P, Mikikian M, Thomann A-L, Brault P. PdPt catalyst synthesized using a gas aggregation source and magnetron sputtering for fuel cell electrodes. Journal of Physics D: Applied Physics, 2015, 48:475302

[7] Kylián O, Valeš V, Polonskyi O, Pešička J, Čechvala J, Solař P, Choukourov A, Slavínská D and Biederman H. Deposition of Pt nanoclusters by means of gas aggregation cluster source. Material Letters, 2012, 79:229–231

[8] Watanabe Y, Wu X, Hirata H and Isomura N. Size-dependent catalytic activity and geometries of size-selected Pt clusters on TiO2(110) surfaces. Catalysis Science & Technolology, 2011, 1:1490–1495

[9] Quesnel E, Pauliac-Vaujour E and Muffato V. Modeling metallic nanoparticle synthesis in a magnetron-based nanocluster source by gas condensation of a sputtered vapor. Journal of Applied Physics, 2010,107:054309

[10] Ayesh A I, Thaker S, Qamhieh N and Ghamlouche H. Size-controlled Pd nanocluster grown by plasma gas-condensation method. Journal of Nanoparticle Research, 2011, 13:1125–1131

[11] Drabik M, Choukourov A, Artemenko A, Polonskyi O, Kylian O, Kousal J, Nichtova L, Cimrova V, Slavinska D and Biederman H. Structure and Composition of Titanium Nanocluster Films Prepared by a Gas Aggregation Cluster Source. Journal of Physical Chemistry C, 2011, 115:20937–20944

[12] Gojdka B, Hrkac V, Strunskus T, Zaporojtchenko V, Kienle L and Faupel F. Study of cobalt clusters with very narrow size distribution deposited by high-rate cluster source. Nanotechnology, 2011, 22:465704

[13] Bouchat V, Feron O, Gallez B, Masereel B, Michiels C, Vander Borght T and Lucas S. Carbon nanoparticles synthesized by sputtering and gas condensation inside a nanocluster source of fixed dimension. Surface and Coatings Technology, 2011, 205:S577–S581

[14] Ten Brink G H, Krishnan G, Kooi B J and Palasantzas G. Copper nanoparticle formation in a reducing gas environment. Journal of Applied Physics, 2014, 116:104302

[15] Koch S A, Palasantzas G, Vystavel T, De Hosson J Th M, Binns C and Louch S. Magnetic and structural properties of Co nanocluster thin films. Physical Review B, 2005, 71:085410

[16] Spadaro M C, D'Addato S, Gasperi G, Benedetti F, Luches P, Grillo V, Bertoni G and Valeri S. Morphology, structural properties and reducibility of size-selected CeO2− x nanoparticle films. Beilstein Journal of Nanotechnology, 2015,6:60–67

[17] D'Addato S, Spadar M C, Luches P, Grillo V, Frabboni S, Valeri S, Ferretti A M, Capetti E and Ponti A. Controlled growth of Ni/NiO core–shell nanoparticles: Structure, morphology and tuning of magnetic properties. Applied Surface Science, 2014, 306: 2-6

[18] Polonskyi O, Ahadi AM, Tilo P, Fujioka K, Abraham JW, Vasiliauskaite E, Hinz A, Strunskus T, Wolf S, Bonitz M, Kersten H, and Faupel F. Plasma based formation and deposition of metal and metal oxide nanoparticles using a gas aggregation source, The European Physical Journal D, 2018, 72:93; and references therein

[19] Liang T, Shin YK, Cheng YT, Yilmaz DE, Vishnu KG, Verners O, Zou C, Phillpot SR, Sinnott SB and van Duin ACT. Reactive Potentials for Advanced Atomistic Simulations. Annual Review of Materials Research, 2013, 43:109–129

[20] Hu W, Li GX, Chen JJ, Huang FJ, Wu Y, Yuan SD, Zhong L, Chen YQ. Enhanced catalytic performance of a PdO catalyst prepared via a two-step method of in situ reduction-oxidation. Chem Commun (Camb). 2017 Jun 1;53(45):6160-6163

[21] Huang F, Chen J, Hu W, Li G, Wu Y, Yuan S, Zhong L, Chen Y, Pd or PdO: Catalytic active site of methane oxidation operated close to stoichiometric air-to-fuel for natural gas vehicles, Applied Catalysis B: Environmental 219 (2017) 73–81.

[22] Liang, X.; Liu, C. -J.; Kuai, P. Selective Oxidation of Glucose to Gluconic Acid over Argon Plasma Reduced Pd/Al_2O_3. Green Chem. 2008, 10, 1318–1322.

[23] Simões, M.; Baranton, S.; Coutanceau, C. Electrochemical valorization of glycerol. ChemSusChem 2012, 5, 2106 – 2124.

[24] Zalineeva, A.; Padilla, M.; Martinez, U.; Serov, A.; Artyushkova, K.; Baranton, S.; Coutanceau, C.; Atanassov, P. B. Self-supported Pd-Bi Catalysts for the Electrooxidation of Glycerol in Alkaline Media. J. Am. Chem. Soc. 2014, 136, 3937 – 3945.

[25] Song S, Wang K, Yan L, Brouzgouc A, Zhang Y, Wang Y, Tsiakaras P, Ceria promoted Pd/C catalysts for glucose electrooxidation in alkaline Media, Applied Catalysis B: Environmental 176–177 (2015) 233–239.

[26] Senftle TP, Meyer RJ, Janik MJ, and van Duin ACT. Development of a ReaxFF potential for Pd/O and application to palladium oxide formation, The Journal of Chemical Physics, 2013, 139:044109

[27] Graves D, Brault P, Molecular dynamics for low temperature plasma-surface interaction studies, Journal of Physics D: Applied Physics, 2009, 42:194011

[28] S. Plimpton, Fast Parallel Algorithms for Short-Range Molecular Dynamics. Journal of Computational Physics, 1995, 117:1-19